Planetary and Space Science 59 (2011) 1654–1658

Contents lists available at ScienceDirect

Planetary and Space Science

journal homepage: www.elsevier.com/locate/pss

Rapid Communication

# Mapping iron abundances on the surface of Mercury: Predicted spatial resolution of the MESSENGER Gamma-Ray Spectrometer

Patrick N. Peplowski [a,*], David T. Blewett [a], Brett W. Denevi [a], Larry G. Evans [b], David J. Lawrence [a], Larry R. Nittler [c], Edgar A. Rhodes [a], Christina M. Selby [a], Sean C. Solomon [c]

[a] Johns Hopkins University Applied Physics Laboratory, Laurel, MD 20723, USA
[b] Computer Sciences Corporation, Lanham, MD 20706, USA
[c] Department of Terrestrial Magnetism, Carnegie Institution of Washington, Washington, DC 20015, USA

ARTICLE INFO

*Article history:*
Received 4 February 2011
Received in revised form
2 June 2011
Accepted 3 June 2011
Available online 12 June 2011

*Keywords:*
Mercury
Gamma-ray spectrometry
Iron
MESSENGER

ABSTRACT

To illustrate the spatial resolution of measurements of Mercury's surface elemental composition by the Gamma-Ray Spectrometer on the MESSENGER spacecraft after one year of orbital observations, we have simulated a global coverage map of the 846-keV iron gamma-ray count rate. The simulated map suggests that distinct geologic units larger than 800 km in horizontal dimension will be discernable when the difference in Fe abundance between adjacent geologic units exceeds 4 wt%. These results imply that the MESSENGER Gamma-Ray Spectrometer dataset will provide useful information for regional geological studies of the surface of Mercury.

© 2011 Elsevier Ltd. All rights reserved.

## 1. Introduction

The MErcury Surface, Space ENvironment, GEochemistry, and Ranging (MESSENGER) spacecraft is en route to the planet Mercury to begin the first orbital exploration of the innermost planet in March 2011 (Solomon et al., 2007). The MESSENGER spacecraft carries a Gamma-Ray Spectrometer (GRS), one of two sensors on the Gamma-Ray and Neutron Spectrometer instrument, for the purpose of measuring gamma-ray emissions from the planet's surface (Goldsten et al., 2007). Analysis of data from MESSENGER's three Mercury flybys has already provided preliminary measurements of the global abundances of Fe, Si, and K (Rhodes et al., 2009). Improved global averages of elemental abundances will certainly be achievable after successful completion of the primary one-year mission. Less certain is the ability of the GRS to produce maps of surface composition with sufficient statistical significance and spatial resolution to resolve individual geologic units.

In this paper we simulate the spatial resolution of the GRS and its ability to resolve differences in Fe content among distinct geologic units. The surface Fe abundance is particularly important, as observations of surface reflectance spectra suggest that Mercury's crustal silicates have a low FeO content relative to surface materials on the other terrestrial planets (e.g., Boynton et al., 2007; McClintock et al., 2008); this is despite the fact that the planet has the highest uncompressed density of any of the terrestrial planets and thus must be metal rich (Solomon et al., 2007). MESSENGER Neutron Spectrometer (NS) measurements during the Mercury flybys indicate that the neutron-absorbing elements Fe and Ti are present on Mercury's surface at combined levels comparable to those of several lunar mare regions (Lawrence et al., 2010). From these two sets of observations, it has been suggested that Fe at Mercury's surface does not reside primarily in silicates but rather in Fe- and Ti-bearing oxides, postulated to be present in variable amounts as a spectrally neutral, low-reflectance component of Mercury surface material (Robinson et al., 2008; Denevi and Robinson, 2008; Denevi et al., 2009). Given Mercury's unusually high bulk density as well as its close proximity to the Sun, understanding the surface composition of Mercury is crucial for testing planetary composition models and by extension theories for the formation of the inner planets (e.g., Taylor and Scott, 2003). Additionally, maps of the surface Fe content and its regional variations will contribute to our understanding of the geologic processes on Mercury.

## 2. Gamma-ray spectrometry

Gamma-ray spectrometry of stable elements is possible because of the interactions between high-energy galactic cosmic ray (GCR) protons and a planetary surface. High-energy protons

* Corresponding author. Tel.: +1 240 228 3979.
*E-mail address:* Patrick.Peplowski@jhuapl.edu (P.N. Peplowski).

0032-0633/$ - see front matter © 2011 Elsevier Ltd. All rights reserved.
doi:10.1016/j.pss.2011.06.001

produce spallation neutrons as they interact with the planetary surface, neutrons that subsequently excite nuclei via neutron inelastic scattering and neutron capture (Prettyman, 2006; Brückner and Masarik, 1997; Reedy, 1978). These excited nuclei decay back to stability via gamma-ray emission, and the energy of the emitted gamma ray is element-specific. Observing this characteristic radiation from orbit with a gamma-ray spectrometer, combined with knowledge of the incident proton flux and instrument response, allows for the determination of the surface composition to depths of tens of centimeters. In the case of Fe, the isotope $^{56}$Fe is excited primarily via neutron inelastic scattering with a well-known reaction probability to the 846-keV excited nuclear state. The subsequent decay of $^{56}$Fe back to a stable state via the emission of an 846-keV gamma ray is a clear indicator of its presence. Because $^{56}$Fe constitutes 91.8% of all naturally occurring Fe, measurement of the 846-keV gamma-ray flux can be used to determine the total Fe content of the surface (Reedy, 1978; Brückner and Masarik, 1997).

Gamma-ray spectrometry is inherently statistics limited, and its signal is inversely proportional to the square of the sensor altitude. As a result, the highly eccentric orbit of the MESSENGER spacecraft limits the ability of the GRS to create global gamma-ray count-rate maps of the surface of Mercury. MESSENGER's nominal orbit has a period of 12 h, a minimum periapsis altitude of approximately 200 km, and an apoapsis altitude of approximately 15,000 km (Fig. 1). To maintain a favorable signal-to-background ratio, MESSENGER GRS data used for analysis will be generally limited to those collected at altitudes lower than the planet's radius of 2440 km, equivalent to less than 2 h per orbit.

The spatial resolution of the GRS, meaning its ability to resolve spatially- and compositionally-distinct regions from each other, is also a function of spacecraft altitude. Analysis of data from the Lunar Prospector (LP) GRS revealed that the spatial response function at low altitudes for an un-collimated gamma-ray sensor is well modeled by a kappa function (Lawrence et al., 2003):

$$w(D,h) = A\left[1+(D^2)/(2\sigma(h)h^2)\right]^{(-\kappa(h)-1)} \quad (1)$$

where $D$ is the distance from the sub-spacecraft point in km, $h$ is the altitude in km, A is a normalization factor, $\sigma$ is the width of the kappa function in km, and $\kappa$ is the tail parameter in km. The quantities $\sigma$ and $\kappa$ vary with altitude as

$$\sigma(h) = 0.704h + 1.39 \quad (2)$$

$$\kappa(h) = -4.87 \times 10^{-4}h + 0.631 \quad (3)$$

On the basis of experience with the LP GRS, the kappa function is used here to calculate the spatial resolution of the MESSENGER GRS.

Given the relationship between spatial resolution and altitude, coupled with the highly eccentric orbit of the MESSENGER spacecraft, producing a map with a spatial resolution sufficient to resolve individual geologic units requires limiting the data to those acquired at a substantially lower maximum spacecraft altitude than one Mercury radius. For this study we use a maximum altitude of 800 km. This condition is met for approximately 30 min of each 12 h orbit (see Fig. 1), and spatial coverage is limited to areas north of 20 °N. Fortunately, this portion of Mercury's surface includes many features of geological interest, including the 1550-km-diameter Caloris impact basin, centered near 30 °N, 165 °E.

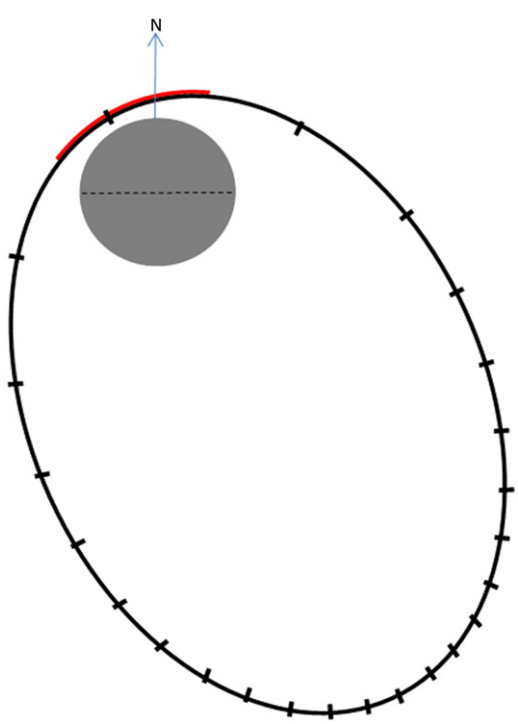


**Fig. 1.** Illustration of the orbit of MESSENGER (to scale) during the spacecraft's one-year primary mission at Mercury (radius 2440 km). The periapsis altitude is approximately 200 km, the orbital period is 12 h, and the tick marks are at 30-min intervals. The red line shows the portion of the orbit for which the GRS data can be used to map surface composition at high resolution for the purpose of this work, i.e., when the altitude is less than 800 km, which amounts to approximately 30 min in each 12-h orbit. (For interpretation of the references to color in this figure legend, the reader is referred to the web version of this article).

## 3. Mercury terrain map and surface Fe abundance

The ability of the GRS to distinguish the elemental composition of the plains that infill the Caloris basin, or the composition of any other geologic feature, from the rest of Mercury's surface would provide an important input to regional geochemical studies of the planet's geological evolution. Spatially resolving geologic features in GRS data is dependent on the spacecraft altitude, the size of the features, and their relative composition. Although the composition of the surface of Mercury is only loosely constrained at present, examination of lateral variations in reflectance and color of surface materials from MESSENGER and Mariner 10 images reveal the presence of mappable regions of distinctive surface composition (Denevi et al., 2009). Because spectral reflectance properties can be correlated to Fe content with additional assumptions, the spectral properties of these regions can be used to estimate Fe abundances for the purpose of simulating the performance of the GRS. The actual surface Fe contents will certainly vary from the estimates made here, but the ability of the GRS to discriminate among geologic features on the basis of their sizes and relative Fe contents, and not the absolute surface Fe abundances, can be demonstrated. The MESSENGER GRS is also sensitive to the presence of a number of other elements, for instance, Si and K, but these elements do not directly influence the spectral properties of the surface, so we currently have no way of constraining their relative variations across the surface.

The Mariner 10 and MESSENGER flybys of the planet Mercury have provided near-global imaging coverage of the surface, revealing many regions that have distinctive reflectance and color characteristics (Robinson and Lucey, 1997; Robinson et al., 2008; Murchie et al., 2008; Denevi et al., 2009). Smooth plains cover approximately 40% of the surface and are divided into three sub-types: high-reflectance red plains (HRP), intermediate plains (IP), and low-reflectance blue plains (LBP). Intermediate terrain (IT) includes areas with high crater density and has spectral properties similar to the global mean. Low-reflectance material (LRM) comprises at least 15% of the surface and tends to be concentrated in crater and basin ejecta.

The Fe contents of these terrain types are unknown. Nonetheless, Earth-based measurements and observations by the MESSENGER spacecraft can be used to assign approximate Fe abundance values. Only a few Earth-based spectral reflectance measurements have resolved a weak 1-μm absorption band (Warell and Blewett, 2004; Warell et al., 2006), originating from an electronic transition in $Fe^{2+}$ when bound to O, and none of the spatially resolved reflectance measurements obtained by MESSENGER have shown such an absorption feature, suggesting that surface silicates contain at most a few weight percent FeO (Boynton et al., 2007; McClintock et al., 2008). Earth-based thermal emission measurements made at microwave wavelengths indicate that the surface is 40% more transparent than the lunar highlands, also supporting the inference of a low Fe content (Mitchell and de Pater, 1994). Any estimates of the surface Fe abundance should ensure that the total Fe content is consistent with these observations.

Fe- and Ti-bearing oxides, such as ilmenite ($FeTiO_3$), have been proposed as candidates for a spectrally neutral, low-reflectance material that could vary in abundance sufficiently to account for the range of color and reflectance seen across Mercury's surface (Rava and Hapke, 1987; Denevi and Robinson, 2008; Robinson et al., 2008; Denevi et al., 2009; Riner et al., 2010). Comparisons of laboratory spectra of ilmenite to the spectral properties of the IT are consistent with up to 22 weight percent (wt%) ilmenite (Denevi et al., 2009), corresponding to $\leq 8$ wt% Fe. Additionally, IT was the terrain type primarily sampled by the MESSENGER GRS and NS during the three flybys. Analysis of the GRS data suggests that the Fe abundance is $7.0 \pm 3.4$ wt% (Rhodes et al., 2009). Analysis of the NS data suggests that the Fe+Ti abundance is between 7 and 18 wt% (Lawrence et al., 2010), consistent with the GRS Fe abundance measurement. Accordingly, a value of 5 wt% Fe is assigned to the IT for the calculations in the paper, consistent with the NS and GRS measurements as well as with indications from spectral reflectance measurements of a low FeO concentration in surface silicates. Areas that were not mapped by Denevi et al. (2009), as well as regions where observing conditions did not allow for a determination of the photometric properties, are assumed to be equivalent in Fe composition to IT.

LRM, which is seen at Mercury's surface primarily in deposits excavated from depth by impact crater formation, exhibits the lowest reflectance on the planet and a relatively shallow spectral slope. If the low reflectance is due solely to the addition of an opaque oxide, such material could contain up to 58 wt% ilmenite (Denevi et al., 2009) for the most extreme cases, corresponding to an Fe content of $\leq 22$ wt%. A value of 9 wt% Fe is assigned to LRM for the calculations here. This value is consistent with the spectral properties and is conservative with regard to average surface Fe abundance.

For HRP, the relatively high reflectance, steep spectral slope, and lack of a 1-μm band are consistent with a low FeO abundance in silicates and a comparative lack of opaque oxides. Areas mapped as HRP or IP are therefore assigned a value of 1 wt% Fe. Because LBP have spectral properties intermediate between those of HRP/IP and LRM, an Fe abundance of 7 wt% is assigned to this terrain type. From the Mercury spectral unit map (Denevi et al., 2009) and the Fe abundances assigned as described, the distribution of estimated Fe abundances used for the simulation presented here is shown in Fig. 2. These values will be adopted to characterize the ability of MESSENGER GRS observations to discriminate between compositionally varying geologic units, measurements that depend on both the assumed absolute Fe content as well as the relative variations in Fe content between different terrains.

## 4. Methodology

Producing a simulated gamma-ray count-rate map requires four inputs: a surface composition map, estimated gamma-ray fluxes, the GRS instrument response, and a spacecraft ephemeris. The derivation of the adopted map of surface composition has been discussed above. Gamma-ray fluxes are taken from the predictions of Bruckner and Masarik (1997), who calculated the gamma-ray flux for the 846-keV Fe gamma ray at an altitude of 200 km to be 0.092γ/($cm^2$ min wt%). This calculation was for an average GCR proton flux incident on the planet, but in reality the GCR flux varies with solar activity. The flux during MESSENGER orbital operations will thus differ somewhat from these predictions. The GRS instrument response was simulated using the radiation transport code GEANT4 (Agostinelli et al., 2003), the results of which were benchmarked to an extensive set of ground-based instrument calibration measurements. These simulations included the GRS detector as well as the surrounding spacecraft components and were used to produce energy and spatially dependent gamma-ray detection efficiency maps. These efficiency maps included the intrinsic GRS detection efficiency as well as the attenuating effects of spacecraft components surrounding the GRS, which can be seen in Fig. 2 of Goldsten et al. (2007). The average value for the 846-keV photopeak detection efficiency for forward angles ($\theta \leq 90^\circ$) is approximately 13%, where $\theta$ denotes the angle between the GRS pointing axis and the vector from the spacecraft to the sub-spacecraft point. Finally, the

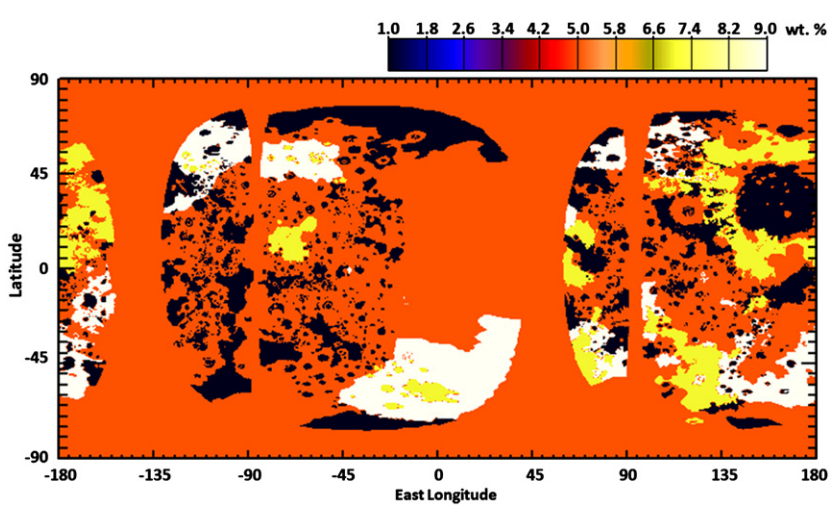


**Fig. 2.** A map of adopted Fe abundance at the surface of Mercury, derived from the mapping of spectral units by Denevi et al. (2009) and an assignment of Fe abundances (wt%) by unit type as discussed in the text. One particular region of interest, the Caloris basin, is the large-diameter (1550 km), low-Fe-content feature located at 30 °N and 165 °E.

spacecraft ephemeris was produced by the MESSENGER science operations planning tool SciBox (Winters et al., 2007). SciBox ephemeris outputs include the spacecraft altitude as well as the location of the sub-spacecraft point on the surface of Mercury, at 30 s intervals for the entire one-year mission.

The process of creating a predictive map of the GRS-measured Fe count rate begins with the adopted map of surface Fe abundance in Fig. 2. The resolution of the map must be convolved with the altitude-dependent GRS spatial resolution, described by the kappa function (Eq. (1)), to determine the Fe abundance as observed by the GRS. The GRS spatial response is calculated using the altitude-dependent kappa function and the average altitude over a given point on the surface from the SciBox ephemeris. This calculation yields a position-dependent map of the spatial resolution for the one-year primary mission. The effective Fe abundance at the surface for any given point, as seen by the GRS, is determined by sampling the Fe composition map (Fig. 2) over the spatial resolution at that point and weighing by the distance from sub-nadir-point-dependent kappa function to determine the surface composition as seen by the GRS. The larger the spatial resolution at a given point, the larger the area sampled by the GRS. The resulting product is a processed surface composition map whose spatial resolution has been filtered by the resolution of the GRS.

The next step is to simulate the altitude- and surface-composition-dependent gamma-ray flux at the GRS. The estimated gamma-ray flux is $0.092\gamma/(\text{cm}^2\,\text{min wt\%})$ at 200 km (Brückner and Masarik, 1997). From SciBox, the position of the spacecraft over the surface and the spacecraft altitude are known for the entire mission. The Fe abundance at the sub-spacecraft point is taken from the filtered map. This abundance is multiplied by the estimated flux and corrected for the spacecraft altitude to determine the average flux at the spacecraft.

The measured gamma-ray flux is then calculated by correcting for the detector area of 19.6 $\text{cm}^2$, the intrinsic detection efficiency at 846 keV, and the attenuating effect of spacecraft components. The attenuation correction is necessary because the GRS is an omnidirectional sensor, but much of the viewing geometry is partially obstructed by spacecraft components, which has the effect of reducing the likelihood that a gamma ray will reach the GRS. The attenuation correction is dependent on the spacecraft attitude, but for this study an attitude-averaged attenuation is used. Similarly, the intrinsic detector efficiency is a function of the incident gamma-ray angle, but the average efficiency over expected orientations is used here. Use of averaged attenuation and efficiency values is justified at this stage, as changes to the science operations will likely result in different spacecraft attitudes than in the pre-orbit plan.

The statistical variation in GRS measurements is estimated by assuming that the count rate will follow a Poisson distribution, the standard assumption for counting experiments for which the data represent the number of events observed within a given time (e.g., Bevington and Robinson, 2003). This assumption is also supported by analysis of the LP GRS data, the statistical variation of which was confirmed to follow a Poisson distribution (Lawrence et al., 2000). Finally, the statistics-corrected count rate is normalized to 200 km altitude in order to remove the altitude dependence, which would otherwise dominate the simulation and obscure any differences in count rate due to changes in the surface Fe abundance. The data are then smoothed and rebinned into $2.5^\circ \times 2.5^\circ$ bins, the results of which are shown in Fig. 3.

## 5. Results

A simulated map of the MESSENGER GRS-measured 846-keV Fe gamma-ray average count rate is shown in Fig. 3, and it can be compared to the adopted Fe abundance map in Fig. 2. To optimize spatial resolution, an upper altitude cut-off of 800 km was used, limiting surface coverage to regions north of $20^\circ$ N. The average gamma-ray count rate varies from 1.3 to 2.3 counts per minute, extremes that correspond to regions of low and high Fe abundance, respectively. Geologic units mapped on the basis of spectral type (Denevi et al., 2009) are clearly discernable in the GRS map, suggesting that gamma-ray data can contribute to regional geologic studies of Mercury.

A number of assumptions went into the production of the simulated Fe gamma-ray count-rate map. The GRS instrument response functions are grounded in instrument calibration data, but the assumed values are for a spatially averaged response. A bias in the spacecraft orientation, such as if a large fraction of data were collected at an attitude with increased gamma-ray attenuation, could modify the simulated map. Additionally, it has been assumed here that the signal-to-background ratio will be sufficient to determine the 846-keV gamma-ray count rate from the spectra. This assumption requires that the 846-keV peak has sufficient signal-to-noise relative to the background continuum to be positively identified, and that the contributions of any interference peaks can be accurately removed.

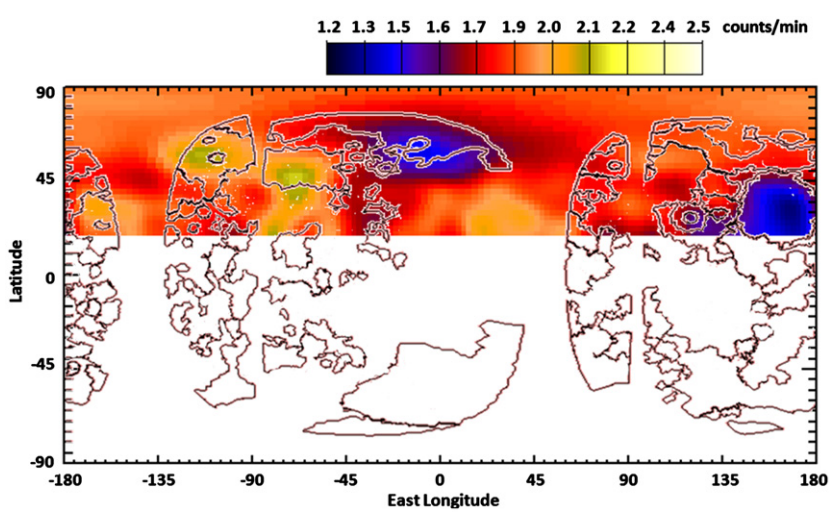


**Fig. 3.** A simulated map of the average 846-keV gamma-ray count rate as measured by MESSENGER's Gamma-Ray Spectrometer during the one-year primary mission. The contours outline the spectral units from Fig. 2 with Fe abundance values in excess of 3 and 6 wt% and units with horizontal extent greater than a few hundred kilometers. The observed correlation between the adopted Fe abundance map and the simulated map suggests that distinct geologic units will be discernable over the course of the MESSENGER mission.

Analysis of the flyby data (e.g., Rhodes et al., 2009) suggests that the 846-keV Fe peak can be resolved from interference peaks as well as the background continuum, so this requirement will be met during MESSENGER's orbital observations. We also assume that the gamma-ray spectra continuum will be well constrained around the 846-keV peak, and that errors in fitting this continuum will be small compared to the statistical error of the 846-keV count rate. The most significant assumption is the assignment of average Fe abundances by spectral unit type, as such assignments have considerable uncertainties.

The simulated map suggests that, regardless of the precise abundances, large regional units will be discernable if they differ in Fe abundance sufficiently from their surroundings. In order to determine the statistical significance with which regions like the plains interior to the Caloris basin can be discriminated from their surroundings, the total 846-keV Fe gamma-ray counts in a given region must be determined. This is accomplished by multiplying the average count rate from Fig. 3 by the total measurement time for each $2.5^\circ \times 2.5^\circ$ pixel. The count total for a region is then determined by summing the total counts from each pixel within its borders. In the case of the Caloris basin, the total number of measured gamma-rays is $1804 \pm 42$. A region of equal area 45° west to the west of Caloris yields $2029 \pm 45$ total counts, a difference greater than five standard deviations from the Caloris basin value. The relative difference in Fe abundance between these two regions is approximately 4 wt%, so we conclude that the MESSENGER GRS will be able to distinguish neighboring geologic features when their diameters exceed 1500 km and their relative Fe contents differ by at least 4 wt%. Analyses for smaller regions with similar abundance differences suggest that the GRS will be able to discriminate between regions as small as 800 km in diameter with a statistical significance greater than three standard deviations.

Careful comparison of the simulated gamma-ray map in Fig. 3 to the assumed Mercury surface Fe composition map in Fig. 2 reveals that the simulated measurements in most regions correlate with the input Fe concentration map. For Caloris basin, one of the best examples of this spatial correlation, low gamma-ray count-rate region corresponds closely to the input Fe abundance map. In contrast, some count rate enhancements show apparent offsets from their corresponding regions on the composition map. For instance, the center of the measured LBP region located at $30^\circ$ N and $-155^\circ$ E is shifted eastward of the corresponding geologic unit, centered at $-165^\circ$E. Such apparent offsets can occur when the GRS spatial footprint is larger than the geologic units being measured. Because the gamma-ray count-rate map is a spatial convolution of sub-footprint-sized regions with different Fe abundances, the resulting map might not always appear to represent the spatial Fe abundance of a given region. This kind of apparent offset has been observed in gamma-ray data from the LP mission, when the spatial resolution of the LP Gamma-Ray Spectrometer was larger than thorium-rich features in the Hansteen Alpha region of the Moon (Lawrence et al., 2005; Hagerty et al., 2006). Forward modeling of gamma-ray transport from the surface to the instrument resolved the apparent spatial offset at Hansteen Alpha, and similar forward modeling analyses will likely be applied to the MESSENGER GRS data. In all cases, these results indicate that statistically significant mapping of MESSENGER GRS data is possible and will produce geologically useful results.

## Acknowledgments

The MESSENGER project is supported by the NASA Discovery Program under contracts NASW-00002 to the Carnegie Institution of Washington and NAS5-97271 to the Johns Hopkins University Applied Physics Laboratory. Financial support from the MESSENGER Participating Scientist Program is also acknowledged.

## References

Agostinelli, S., et al., 2003. GEANT4—a simulation toolkit. Nucl. Instrum. Methods A 506, 250–303.
Bevington, P.R., Robinson, D.K., 2003. Data Reduction and Error Analysis for the Physical Sciences, 3rd ed. McGraw-Hill, Boston, 320 pp.
Boynton, W.V., Sprague, A.L., Solomon, S.C., Starr, R.D., Evans, L.G., Feldman, W.C., Trombka, J.I., Rhodes, E.A., 2007. MESSENGER and the chemistry of Mercury. Space Sci. Rev. 131, 85–104.
Brückner, J., Masarik, J., 1997. Planetary gamma-ray spectroscopy of the surface of Mercury. Planet. Space Sci. 45, 39–48.
Denevi, B.W., Robinson, M.S., 2008. Mercury's albedo from Mariner 10: implications for the presence of ferrous iron. Icarus 197, 239–246.
Denevi, B.W., Robinson, M.S., Solomon, S.C., Murchie, S.L., Blewett, D.T., Domingue, D.L., McCoy, T.J., Ernst, C.M., Head, J.W., Watters, T.R., Chabot, N.L., 2009. The evolution of Mercury's crust: a global perspective from MESSENGER. Science 324, 613–618.
Goldsten, J.O., Rhodes, E.A., Boynton, W.V., Feldman, W.C., Lawrence, D.J., Trombka, J.I., Smith, D.M., Evans, L.G., White, J., Madden, N.W., Berg, P.C., Murphy, G.A., Gurnee, R.S., Strohbehn, K., Williams, B.D., Schaefer, E.D., Monaco, C.A., Cork, C.P., Eckels, J.D., Miller, W.O., Burks, M.T., Hagler, L.B., DeTeresa, S.J., Witte, M.C., 2007. The MESSENGER Gamma-Ray and Neutron Spectrometer. Space Sci. Rev. 131, 339–391.
Hagerty, J.J., Lawrence, D.J., Hawke, B.R., Vaniman, D.T., Elphic, R.C., Feldman, W.C., 2006. Refined thorium abundances for lunar red spots: implications for evolved, nonmare volcanism on the Moon. J. Geophys. Res. 111, E06002. doi:10.1029/2005JE002592.
Lawrence, D.J., Feldman, W.C., Barraclough, B.L., Binder, A.B., Elphic, R.C., Maurice, S., Miller, M.C., Prettyman, T.H., 2000. Thorium abundances on the lunar surface. J. Geophys. Res. 105, 20307–20331.
Lawrence, D.J., Elphic, R.C., Feldman, W.C., Prettyman, T.H., Gasnault, O., Maurice, S., 2003. Small-area thorium features on the lunar surface. J. Geophys. Res. 108 (E9), 5102. doi:10.1029/2003JE002050.
Lawrence, D.J., Hawke, B.R., Hagerty, J.J., Elphic, R.C., Feldman, W.C., Prettyman, T.H., Vaniman, D.T., 2005. Evidence for high-Th, evolved lithology on the Moon at Hansteen Alpha. Geophys. Res. Lett. 32, L07201. doi:10.1029/2004GL022022.
Lawrence, D.J., Feldman, W.C., Goldsten, J.O., McCoy, T.J., Blewett, D.T., Boynton, W.V., Evans, L.G., Nittler, L.R., Rhodes, E.A., Solomon, S.C., 2010. Identification and measurement of neutron-absorbing elements on Mercury's surface. Icarus 209, 179–194.
McClintock, W.E., Izenberg, N.R., Holsclaw, G.M., Blewett, D.T., Domingue, D.L., Head III, J.W., Helbert, J., McCoy, T.J., Murchie, S.L., Robinson, M.S., Solomon, S.C., Sprague, A.L., Vilas, F., 2008. Spectroscopic observations of Mercury's surface reflectance during MESSENGER's first Mercury flyby. Science 321, 62–65.
Mitchell, D.L., de Pater, I., 1994. Microwave imaging of Mercury's thermal emission at wavelengths from 0.3 to 20.5 cm. Icarus 110, 2–32.
Murchie, S.L., Watters, T.R., Robinson, M.S., Head, J.W., Strom, R.G., Chapman, C.R., Solomon, S.C., McClintock, W.E., Prockter, L.M., Domingue, D.L., Blewett, D.T., 2008. Geology of the Caloris basin, Mercury: a view from MESSENGER. Science 321, 73–76.
Prettyman, T.H., 2006. Remote chemical sensing using nuclear spectroscopy. In: McFadden, L.-A., Weissman, P.R., Johnson, T.V. (Eds.), Encyclopedia of the Solar System, 2nd ed. Academic Press, Amsterdam, pp. 765–787.
Rava, B., Hapke, B., 1987. An analysis of the Mariner 10 color ratio map of Mercury. Icarus 71, 397–429.
Reedy, R.C., 1978. Planetary gamma-ray spectroscopy. In: Proceedings of the Ninth Lunar and Planetary Science Conference, pp. 2961–2984.
Rhodes, E.A., Evans, L.G., Goldsten, J.O., Nittler, L.R., Starr, R.D., Boynton, W.V., Sprague, A.L., Lawrence, D.J., Solomon, S.C., MESSENGER Team, 2009. Gamma-ray spectrometer measurements at Mercury during the MESSENGER flybys. Eos Trans. Am. Geophys. Union 90 (52), Fall Meet. Suppl., abstract P21A-1194.
Riner, M.A., McCubbin, F.M., Lucey, P.G., Taylor, G.J., Gillis-Davis, J.J., 2010. Mercury surface composition: integrating petrological modeling and remote sensing data to place constraints on FeO abundance. Icarus 209, 301–313.
Robinson, M.S., Lucey, P.G., 1997. Recalibrated Mariner 10 color mosaics: implications for Mercurian volcanism. Science 275, 197–200.
Robinson, M.S., Murchie, S.L., Blewett, D.T., Domingue, D.L., Hawkins III, S.E., Head, J.W., Holsclaw, G.M., McClintock, W.E., McCoy, T.J., McNutt Jr., R.L., Prockter, L.M., Solomon, S.C., Watters, T.R., 2008. Reflectance and color variations on Mercury: regolith processes and compositional heterogeneity. Science 321, 66–69.
Solomon, S.C., McNutt, R.L., Gold, R.E., Domingue, D.L., 2007. MESSENGER mission overview. Space Sci. Rev. 131, 3–39.
Taylor, G.J., Scott, E.R.D., 2003. Mercury. In: Davis, A.M. (Ed.), Meteorites, Comets, and Planets. Treatise on Geochemistry, vol. 1. Elsevier, Amsterdam, pp. 477–485.
Warell, J., Blewett, D.T., 2004. Properties of the Hermean regolith. V. New optical reflectance spectra, comparison with lunar anorthosites, and mineralogical modeling. Icarus 168, 257–276.
Warell, J., Sprague, A.L., Emery, J.P., Kozlowski, R.W.H., Long, A., 2006. The 0.7–5.3 μm IR spectra of Mercury and the Moon: evidence for high-Ca clinopyroxene on Mercury. Icarus 180, 281–291.
Winters, H.L., Domingue, D.L., Choo, T.H., Espiritu, R., Hash, C., Malaret, E., Mick, A.A., Skura, J.P., Steele, J., 2007. The MESSENGER Science Operations Center. Space Sci. Rev. 131, 601–623.